generate magnetic fields and coronal x-ray emission. A rotation-induced dynamo is needed (*6*). The star VB 8 with spectral type M7 is the star with the latest spectral type that shows quiescent x-ray emission, namely, log (L_x/L_{bol}) $= -2.8$ (where L_x is the x-ray luminosity and L_{bol} is the bolometric luminosity) (*19*). Also, the M8 star VB 10 was detected at log (L_x/L_{bol}) $\simeq -3$, but only during a flare. The quiescent upper limit is log (L_x/L_{bol}) ≤ -4.5 before and after the flare (*20*). In addition, the M6 to M7 T Tauri star V410 x-ray 3 was also detected as an x-ray source (*21*). With a mass of 0.08 to 0.15 $M_\odot$, an age of 10^6 years, and log (L_x/L_{bol}) $= -2.8$ (*22*), it is similar to Cha Hα 1, but slightly more massive. The object 1623-2426, a young BD in ρ Oph (*5*), was not detected in the 33-ks PSPC pointed observation 200045, newly reduced by us (*23*), with the upper limit being log (L_x/L_{bol}) ≤ -3.26, above the value measured for Cha Hα 1.

With an optical magnitude in the V band of 21 magnitudes (*7*), Cha Hα 1 is the optically faintest low-mass object we observed. Yet, it is the x-ray brightest object, and the x-ray to bolometric luminosity relation cannot explain why only Cha Hα 1 is detected in x-rays. It is possible that Cha Hα 1 rotates fast to support a strong dynamo. The spectral resolutions of our observations are too low to determine the rotational velocity. Because ρ Oph 1623-2426 has a mass similar to Cha Hα 1 and is 3 to 10 times older, but it is not detected as an x-ray source, only the combination of a young age ($\leq 3 \times 10^6$ years) and fast rotation (≥ 20 km/s) may allow us to detect x-ray emission from a BD (*24*). Alternative models for BD x-ray emission appear less likely: (i) Flare activity without (or with faint) quiescent emission, for example, due to magnetic field reconnections, as in the late-type star VB 10 (*20*), is not supported by our observations, because we find no evidence for variability in the x-ray emission. (ii) If Cha Hα 1 were a close binary with magnetic field configurations similar to those in x-ray bright, interacting low-mass binaries, it should be brighter in the optical than observed (*7*). (iii) The x-ray emission cannot be linked with any circumstellar material, because we do not see any NIR excess (*7*). Hence, coronal activity appears to be the most plausible explanation for the x-ray emission that is consistent with all the other observational data.

The x-ray detection of Cha Hα 1 suggests that a young BD can support a magnetic corona. Therefore, it may be possible to find more young BDs in star-forming regions as counterparts to faint x-ray sources in x-ray observations with long exposure times. Establishing the BD x-ray luminosity function and estimating the integrated x-ray emission are important for assessing the BD contribution to the diffuse galactic x-ray emission and the baryonic dark matter in the galactic halo.

References and Notes

1. A. Burrows and J. Liebert, *Rev. Mod. Phys.* **65**, 301 (1993); S. R. Kulkarni, *Science* **276**, 1350 (1997).
2. A. Burrows et al., *Nature* **375**, 299 (1995).
3. J. R. Stauffer, D. Hamilton, R. Probst, *Astron. J.* **108**, 155 (1994); R. Rebolo, M. R. Zapatero-Osorio, E. L. Martín, *Nature* **377**, 129 (1995); G. Basri, G. W. Marcy, J. Graham, *Astrophys. J.* **458**, 600 (1996); M. R. Zapatero-Osorio, R. Rebolo, E. L. Martín, *Astron. Astrophys.* **317**, 164 (1997).
4. F. Comerón, G. H. Rieke, P. Claes, J. Torra, R. J. Laureijs, *Astron. Astrophys.* **335**, 522 (1998).
5. K. L. Luhman, J. Liebert, G. H. Rieke, *Astrophys. J.* **489**, L165 (1998).
6. B. Dorman, L. Nelson, W. Chau, *ibid.* **342**, 1003 (1989); F. D'Antona and I. Mazzitelli, *ibid.* **296**, 502 (1985).
7. F. Comerón, G. H. Rieke, R. Neuhäuser, in preparation.
8. S. K. Leggett, F. Allard, G. Berriman, C. C. Dahn, P. H. Hauschildt, *Astrophys. J. Suppl.* **104**, 117 (1996).
9. F. Allard, P. H. Hauschildt, D. R. Alexander, S. Starrfield, *Annu. Rev. Astron. Astrophys.* **35**, 137 (1997).
10. A. Burrows et al., *Astrophys. J.* **491**, 856 (1997); F. D'Antona and I. Mazzitelli, in *Proceedings of the Meeting on Cool Stars in Clusters and Associations*, G. Micela, R. Pallavicini, S. Sciortino, Eds. (Astronomical Society of Italy, Florence, 1997), pp. 807–822; F. D'Antona et al., in preparation; A. Burrows et al., in preparation.
11. J. Trümper, *Adv. Space Res.* **2** (no. 4), 241 (1983); E. Pfeffermann et al., *Proc. SPIE* **733**, 519 (1988).
12. E. D. Feigelson and G. A. Kriss, *Astrophys. J.* **338**, 262 (1989).
13. E. D. Feigelson et al., *ibid.* **416**, 623 (1993).
14. M. Braun, thesis, Friedrich-Schiller Universität, Jena, Germany (1992).
15. J. Liebert et al., in *7th Cambridge Workshop on Cool Stars, Stellar Systems, and the Sun*, vol. 26 of ASP Conference Series, M. S. Giampapa and J. A. Bookbinder, Eds. (ASP, San Francisco, 1992), pp. 282–283.
16. J. D. Kirkpatrick, T. J. Henry, D. W. McCarthy, *Astrophys. J. Suppl.* **77**, 417 (1991); J. D. Kirkpatrick, T. J. Henry, D. A. Simon, *Astron. J.* **109**, 797 (1995).
17. C. F. Prosser, J. R. Stauffer, R. P. Kraft, *Astron. J.* **101**, 1361 (1991); E. L. Martín, R. Rebolo, M. R. Zapatero-Osorio, *Astrophys. J.* **469**, 706 (1996).
18. K. L. Luhman and G. H. Rieke, *Astrophys. J.* **497**, 354 (1998).
19. M. S. Giampapa et al., *ibid.* **463**, 707 (1996).
20. T. Fleming, J. H. M. M. Schmitt, M. S. Giampapa, in preparation.
21. K. M. Strom and S. E. Strom, *Astrophys. J.* **424**, 237 (1994).
22. K. L. Luhman et al., *ibid.* **493**, 909 (1998).
23. A slightly larger x-ray upper limit was reported in (*5*) obtained from the 1σ noise level in the hard band ROSAT map published by S. Casanova et al. [*Astrophys. J.* **439**, 752 (1995)].
24. None of the 11 bona fide BDs published so far, all with ages $\geq 3 \times 10^6$ years and rotational velocities ≥ 20 km/s (as far as known), were detected in x-ray observations (R. Neuhäuser et al., in preparation).
25. W. A. Lawson, E. D. Feigelson, D. P. Huenemoerder, *Mon. Not. R. Astron. Soc.* **280**, 1071 (1996).
26. We are grateful to H. Zinnecker, J. Schmitt, E. Martín, and G. Rieke for useful discussion about BDs, ESO for allocation of telescope time, C. Lidman and G. Carraro for allowing the use of their telescope time, A. Burrows and F. D'Antona for providing their new pre–main-sequence tracks, E. Feigelson for allowing the use of his ROSAT observation, the second processing of which is not yet publicly available, and B. Stelzer and T. Hearty for part of the specific software development. ROSAT is supported by the German government (BMBF/DLR) and the Max-Planck-Society.

6 July 1998; accepted 2 September 1998

Measuring the Spin Polarization of a Metal with a Superconducting Point Contact

R. J. Soulen Jr., J. M. Byers,* M. S. Osofsky, B. Nadgorny, T. Ambrose, S. F. Cheng, P. R. Broussard, C. T. Tanaka, J. Nowak, J. S. Moodera, A. Barry, J. M. D. Coey

A superconducting point contact is used to determine the spin polarization at the Fermi energy of several metals. Because the process of supercurrent conversion at a superconductor-metal interface (Andreev reflection) is limited by the minority spin population near the Fermi surface, the differential conductance of the point contact can reveal the spin polarization of the metal. This technique has been applied to a variety of metals where the spin polarization ranges from 35 to 90 percent: $Ni_{0.8}Fe_{0.2}$, Ni, Co, Fe, NiMnSb, $La_{0.7}Sr_{0.3}MnO_3$, and CrO_2.

A new class of electronics is emerging based on the ability of ferromagnetic metals to conduct spin-polarized currents (*1*). The effectiveness of magnetoelectronics depends on the extent to which a current is spin-polarized. All device designs improve their performance as the spin polarization $P \rightarrow 100\%$. For both scientific and technological reasons it is important to be able to directly and easily measure the electronic spin polarization at the Fermi energy, E_F, of a candidate material.

Unfortunately, determining P at E_F of a ferromagnet (FM) is not easy. A typical transition-metal FM has two components to its electronic structure: narrow d bands that may be fully or partially spin-polarized (due to the on-site exchange energy) and broad s bands with a lesser degree of spin polarization (due to hybridization with the d bands). The quantity P can be defined as

$$P = \frac{N_\uparrow(E_F) - N_\downarrow(E_F)}{N_\uparrow(E_F) + N_\downarrow(E_F)} \quad (1)$$

where $N_\sigma(E)$ is the spin-dependent density of states. The value of P is controlled by the

extent to which these *s* and *d* bands cross the Fermi surface. If the orbital character at the Fermi surface of a FM is primarily *d*-like, then *P* will be high. If, however, the orbital character is *s*-like or *s*-*d*–hybridized, then *P* can be low or high depending on the details of the electronic structure. The magnetization of a material may show that all of the electronic spins associated with the *d* orbitals are aligned but that *P* at E_F can be depressed (*2*). However, metallic oxide FMs, for example, have a greater opportunity for high values of *P* because of the predominance of *d*-orbital character at E_F.

Measuring *P* requires a spectroscopic technique that can discriminate between the spin-up and spin-down electrons near E_F. Spin-polarized photoemission spectroscopy is technically capable of providing the most direct measurement of *P*, but lacks the necessary energy resolution (≈ 1 meV) (*3*). An effective alternative to photoemission is the use of spin-polarized tunneling in a planar junction geometry that does allow the electronic spectrum near E_F to be probed with submillielectron volt energy resolution. Tedrow and Meservey (*4*) pioneered this technique by making FM-superconductor (SC) tunnel junctions and Zeeman splitting the SC's strongly peaked single-particle excitation spectrum by the application of a magnetic field. The resulting spectrum of the SC roughly corresponds to two fully spin-polarized peaks (neglecting spin-orbit coupling effects) that can be used to detect *P* of a current *I* from the FM film. The tunnel junction technique has been successfully used to find *P* for a number of magnetic metals. The drawback of the technique is the constraint of fabricating a layered device consisting of a thin-film FM on top of a uniform oxide layer 10 to 20 Å thick that is formed on top of the SC base. The need for a uniform oxide layer is a severe limitation of the technique because many interesting materials cannot be made within this stringent constraint.

Accordingly, we have developed an approach to measuring *P* of a metal that requires no magnetic field and places no special constraints on a sample; thin films, single crystals, and foils of several metals have been successfully measured. In contrast to the tunnel junctions used by Tedrow and Meservey,

we form a metallic point contact between the sample and a superconductor using a simple mechanical adjustment. Unlike a tunnel junction, a metallic contact allows coherent two-particle transfer at the interface between the normal metal and the SC. The electronic transport properties at the point contact measures the conversion between superconducting pairs and the single-particle charge carriers of the metal.

The conversion of normal current to supercurrent at a metallic interface is called Andreev reflection (*5*) and is a well-known phenomenon in superconductivity. To understand this process, consider Fig. 1A showing an electron in a metal with *P* = 0 propagating toward the interface. For the electron to enter the superconducting condensate and proceed as part of the supercurrent, it must be a member of a pair. The other electron required for the formation of the pair is obtained from the metal, thus leaving behind a hole at the interface. This hole has the opposite momentum of the incident electron and propagates away from the interface. The Andreev reflected holes act as a parallel conduction channel to the initial electron current, doubling the normal-state conductance G_n (where $G = dI/dV$ and *V* is the voltage) of the point contact for applied voltages $eV < \Delta$, where Δ is the superconducting gap at the interface. In an *I-V* measurement, the supercurrent conversion appears as an excess current added to the ohmic response at the interface. We illustrate the effect experimentally in Fig. 1B for a superconducting niobium (Nb) point pressed

into a Cu foil at a temperature of 1.6 K. At low voltage the normalized conductance is indeed twice that of the normal state, and an excess current of ≈ 0.2 mA is present.

The probes for this study were fabricated by mechanically polishing SC rods of superconducting material [Nb and tantalum (Ta)] to a sharp point with progressively finer sandpaper. Examination of the sharpened points with a scanning electron microscope indicated that all were roughly cone shaped and tapered to a rounded end with an approximate radius of 100 μm. However, the extreme portion of the tips was studded with several protrusions that were 1 μm or smaller and likely formed the actual point contact. Positioning and adjustment of the point contact was achieved by simple mechanical means. The tip was attached to a drive shaft vertically positioned above the sample material. The shaft was driven by a micrometer mechanism capable of moving the point linearly by 100 μm per revolution. All of the transport measurements were made with a conventional four-terminal arrangement while the point contact and sample were immersed in a liquid He bath at either 4.2 or 1.6 K. The *dI/dV* data in this study were obtained by standard ac lock-in techniques at a frequency of 2 kHz.

To understand the effect of *P* on the Andreev reflection process, consider Fig. 1A again. Because a superconducting pair is composed of a spin-up and spin-down electron, an incident spin-up electron in the metal requires a spin-down electron to be removed from the metal as well for conversion to
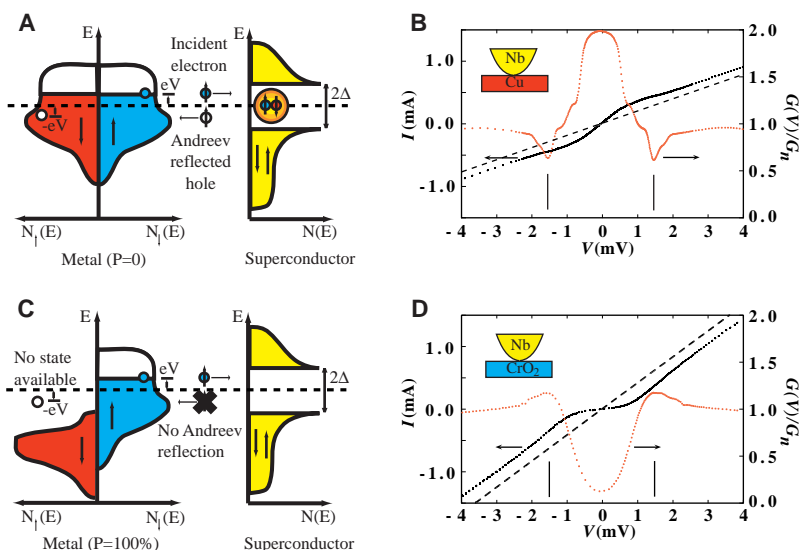
R. J. Soulen Jr., M. S. Osofsky, B. Nadgorny, T. Ambrose, S. F. Cheng, P. R. Broussard, Materials Physics, Naval Research Laboratory, Washington, DC 20375, USA. J. M. Byers, Department of Physics, George Washington University, Washington, DC 20052, and Materials Physics, Naval Research Laboratory, Washington, DC 20375, USA. C. T. Tanaka, J. Nowak, J. S. Moodera, Massachusetts Institute of Technology, Francis Bitter Magnet Laboratory, Cambridge, MA 02139, USA. A. Barry and J. M. D. Coey, Department of Physics, Trinity College, Dublin 2, Ireland.

*To whom correspondence should be addressed. E-mail: byers@foucault.nrl.navy.mil

Fig. 1. Supercurrent conversion at the superconductor-metal interface for spin polarizations of *P* = 0 and *P* → 100%. (**A**) Schematic of the process for *P* = 0 when the Andreev reflection is unhindered by a spin minority population at E_F. The solid circles denote electrons and open circles denote holes. (**B**) Experimental measurement of the *I-V* and differential conductance *dI/dV* at *T* = 1.6 K via a superconducting Nb point contact on Cu. The vertical lines denote the bulk gap of Nb: $\Delta(T = 0)$ = 1.5 meV. The dashed line is the normal state *I-V* for a conductance of G_n = 0.194 ohm^{-1}. (**C**) Schematic of process for *P* → 100% when there is no supercurrent conversion at the interface. (**D**) Experimental *I-V* and *dI/dV* at *T* = 1.6 K via the Nb point contact on CrO_2. The dashed line is the normal state *I-V* for a conductance of G_n = 0.417 ohm^{-1}.

supercurrent. The removal of the spin-down electron leaves a spin-up hole that is Andreev reflected back into the metal. Note that the spin-up hole is the absence of a spin-down electron and so by convention is in the spin-down density of states (DOS) as shown in Fig. 1A. Tracking the spin during Andreev reflection shows that the process is a coherent interspin-subband transfer that is sensitive to the relative electronic spin DOS or P at E_F. If $P = 0$, then the Andreev reflection is unhindered by a lack of spin minority carriers for the formation of pairs to enter a supercurrent. However, if $P = 100\%$ near E_F, as depicted in Fig. 1C, then there are no spin-down states in the metal to provide the other member of the superconducting pair for Andreev reflection. Supercurrent conversion via Andreev reflection at the interface is effectively blocked, allowing only single-particle excitations to contribute to the conductance. These single-particle states necessarily see the gap in the energy spectrum of the SC, thus suppressing the conductance G for $eV < \Delta$.

In Fig. 1D a superconducting Nb point contact is used on an epitaxial film of CrO_2 deposited on an oriented TiO_2 substrate (6). Experimental (7) and theoretical (8) works have suggested that CrO_2 is a half-metallic FM expected to have $P = 100\%$ at E_F. Our results directly confirm this expectation because nearly all of the Andreev reflection has been suppressed, implying almost full spin polarization.

For the cases $P = 0$ and $P = 100\%$, the definition of P is not critical. However, for intermediate spin polarizations more careful consideration must be given to the nature of the experiment. The spin polarization P as written in Eq. 1 is nearly impossible to obtain in a transport experiment, yet transport is really the only means to obtain the needed energy resolution. The results of Tedrow and Meservey for P are more accurately described as a tunneling polarization,

$$P_T = \frac{N_\uparrow(E_F)|T_\uparrow|^2 - N_\downarrow(E_F)|T_\downarrow|^2}{N_\uparrow(E_F)|T_\uparrow|^2 + N_\downarrow(E_F)|T_\downarrow|^2} \quad (2)$$
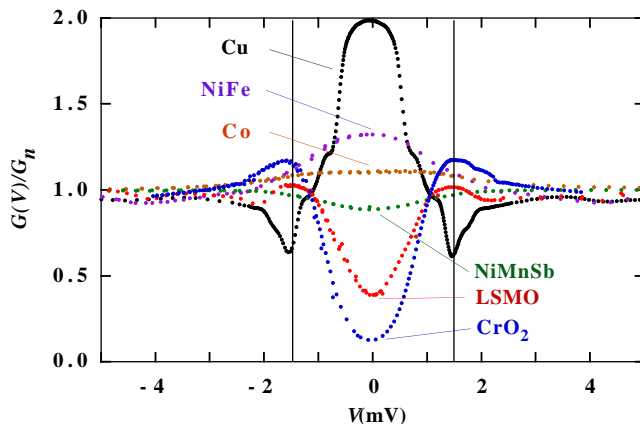
where $T_\uparrow$ and $T_\downarrow$ are spin-dependent tunneling matrix elements. These matrix elements are determined by wave function overlap at the interface and should generally differ for the spin-up and spin-down bands (9). For the point contact measurements reported here (with negligible interfacial scattering) we measure a contact polarization,

$$P_C = \frac{N_\uparrow(E_F)v_{F\uparrow} - N_\downarrow(E_F)v_{F\downarrow}}{N_\uparrow(E_F)v_{F\uparrow} + N_\downarrow(E_F)v_{F\downarrow}} \quad (3)$$

where $v_{F\sigma}$ is the Fermi velocity of the respective band. The appearance of $v_{F\sigma}$ in this expression is expected for a point contact (10) and leads to the observation

$$P_C = \frac{I_\uparrow - I_\downarrow}{I_\uparrow + I_\downarrow} \quad (4)$$

because $I_\sigma \propto v_{F\sigma} N_\sigma(E_F)$. These different but related values for P will be distinguished when necessary hereafter. The point contact technique can measure P of currents characteristic of ballistic transport in the bulk material when interfacial scattering in the point contact is minimal as achieved in this study. From the standpoint of understanding spin-polarized transport and magnetoelectronics in nanostructures, determination of the P_C is more relevant than P of the density of states.

To understand the dI/dV curves in more detail requires a model for Andreev reflection in the presence of a spin-polarized metal. We have developed such a theoretical framework for analyzing the data and extracting P_C by adapting the Blonder-Tinkham-Klapwijk (BTK) theory for conventional Andreev reflection ($P_C = 0$) (11) to the case for spin-polarized materials ($P_C \neq 0$). The BTK theory allows the inclusion of interfacial scattering at the point contact through a parameter Z governed by the ratio of a scattering potential and the Fermi velocity. A ballistic point contact with no scattering has $Z = 0$, whereas a tunnel junction corresponds to the limit $Z \rightarrow \infty$. As Z increases, Andreev reflection at low voltages is suppressed and the characteristic spikes of a tunnel junction develop at $eV = \pm\Delta$. Determining if Z is present is straight-

forward because the conductance peaks that develop at the gap edges are sensitive to the increase in Z at low temperatures T. This study will focus on those point contact configurations where Z is small. For our purposes consider the decomposition of the current through the point contact into

$$I = I_\uparrow + I_\downarrow = 2I_\downarrow + (I_\uparrow - I_\downarrow)$$
$$= I_{unpol} + I_{pol}$$

where the unpolarized current, I_{unpol}, carries no net P and obeys the conventional BTK theory. The remaining current, I_{pol}, carries all of P and as such is entirely a quasiparticle current (because supercurrent can carry no net polarization). This current can be calculated by allowing only non-Andreev processes at the point contact. Within the BTK theory this procedure amounts to setting the Andreev coefficient, $A(E)$, to zero and renormalizing all of the remaining processes to 1 for current conservation. P_C can be extracted from the dI/dV curves by noting that

$$\frac{d}{dV} I(V,T; P_C, Z) =$$

$$(1 - P_C) \frac{d}{dV} I_{unpol}(V, T; Z)$$

$$+ P_C \frac{d}{dV} I_{pol}(V, T; Z) \quad (5)$$

If the interfacial scattering is minimal ($Z \approx 0$), then for $eV \ll \Delta$ and $k_B T \ll \Delta$ (where k_B is Boltzmann's constant) the term

$$\frac{1}{G_n} \frac{d}{dV} I_{unpol} = 2 \text{ and } \frac{d}{dV} I_{pol} = 0$$

to yield

$$\frac{1}{G_n} \frac{dI}{dV} (eV \rightarrow 0, T \rightarrow 0; P_C, Z = 0)$$
$$= 2(1 - P_C) \quad (6)$$

a result anticipated by de Jong and Beenakker (12) in this extreme limit. Under these restrictions, obtaining P_C is straightforward from

Fig. 2. The differential conductance for several spin-polarized metals showing the suppression of Andreev reflection with increasing P_C. The vertical lines denote the bulk gap of Nb: $\Delta(T = 0) = 1.5$ meV.
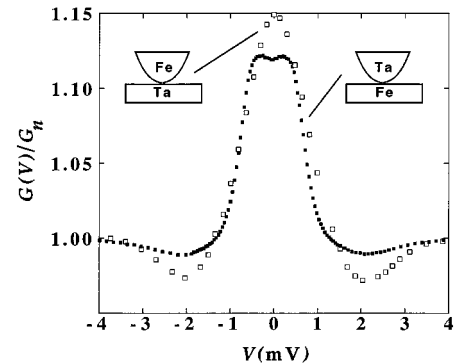
Fig. 3. The differential conductance for a Fe-Ta configuration where Fe is the sample and Ta the point and vice versa. The spin polarization for the Fe ($P_C = 43\%$) is nearly the same in either configuration. Note that $\Delta(T = 0) = 0.7$ meV for Ta.

our technique. When these conditions are relaxed ($Z \neq 0$ and finite T), a numerical fitting procedure over the entire voltage range with our modified form of the BTK model can be used to obtain P_C.

In Fig. 2 we present a series of samples that show varying degrees of P_C to demonstrate the applicability of the superconducting point contact technique. As prescribed by Blonder and Tinkham (13), only data from those point-contact configurations with an ohmic contact resistance $1/G_n$ between 1 and 100 ohms were analyzed. This criterion also helps remove consideration of contacts with too much plastic deformation that causes low contact resistance and heating due to high current densities. For a Sharvin point contact (10) between typical metals (Cu and Nb), this range implies contact areas of $\sim 10^4$ Å^2. Additionally, we include in Fig. 2 only those contacts where the interfacial scattering, Z, appears to be minimal, allowing a direct estimate of P_C by Eq. 6. The dI/dV curves for Cu ($P_C = 0$) and CrO$_2$ ($P_C \approx 100\%$) are reproduced in Fig. 2 for comparison with metals of intermediate P_C. A polycrystalline permalloy (Ni$_{0.8}$Fe$_{0.2}$) film, which was grown by sputtering, showed a P_C of 35%, a value between the differing results of the tunneling technique (4, 14). The spin polarization of permalloy seems to be sensitive to preparation conditions and is capable of significantly higher values (14). Also measured were single-crystal thin films of Fe grown by molecular beam epitaxy (15) and a sputtered polycrystalline Ni film. A representative result for Co foil is shown in Fig. 2, indicating a P_C of 42%. Our measured value is slightly greater than that reported by Tedrow and Meservey ($P_T = 35\%$). Our result for Ni of $P_C = 45\%$ is close to that of the Fe and Co measurements but is different from P_T measured by Tedrow and Merservey ($P_T = 23\%$). However, our value of P_C is not far from more recent measurements of $P_T = 33\%$

(14). The measured spin polarization of Ni and Ni-rich alloys has been shown to be very sensitive to impurities, possibly accounting for the discrepancies observed. Another possible source of disagreement is that the differences in the definition of spin polarization may be more pronounced for Ni compounds.

The three lowest dI/dV curves of Fig. 2 are for compounds that have not been examined by the tunnel junction technique. These materials are easily measured with our point contact technique. A Heusler alloy film, NiMnSb, grown by three-source co-evaporation (description of growth technique to be published), shows a polarization of $P_C = 58\%$ in contrast to expectations that it should be fully spin-polarized (16). Examination of the structure by extended x-ray absorption fine structure spectroscopy showed some segregation of the Sb near the surface of Heusler films grown by this technique (17). A thin film of the colossal magnetoresistance material, La$_{0.7}$Sr$_{0.3}$MnO$_3$, grown by off-axis sputtering (18) showed a P_C of almost 80%, near the value expected from a half-metallic FM with a fully spin-polarized Fermi surface. And finally we show the CrO$_2$ film with close to 100% spin polarization as discussed in Fig. 1D. Although this curve bears some resemblance to a tunnel junction with magnetic impurities, the substantial nonconservation of spectral weight compared to the normal state reveals that the effect is primarily caused by the spin polarization of the CrO$_2$ instead.

To ensure the consistency of our results, we have also studied the effect of reversing the role of the two materials. For example, Fig. 3 compares the conductance curves for two cases: a sharpened Ta point placed in contact with a single-crystal Fe thin film, and a sharpened Fe point placed in contact with a polycrystalline Ta foil. There is no significant difference between the shape of the conductance curves for the two cases, and analysis shows that nearly the same values are ob-

tained for the gap Δ and P_C. The slight difference near zero bias is due to varying amounts of interfacial scattering Z.

Our results are summarized in Table 1 with the materials arranged in ascending values of P_C. In our technique, the deviation from the mean value of polarization P_C (Table 1) is not controlled solely by experimental error because it may be due to the actual distribution of the spin polarization within the sample as well as surface-scattering effects. Nevertheless, the statistical variation is comparable to the tunneling results. The simplicity of our method allows materials not previously measured for spin polarization at E_F (NiMnSb, La$_{0.7}$Sr$_{0.3}$MnO$_3$, and CrO$_2$) to be studied. The point contact technique has the added advantage of providing rapid feedback in the development of spin-polarized materials for magnetoelectronics by making the determination of electronic spin polarization no more difficult than a low-temperature magnetization measurement.

Note added in proof: We have become aware of related work by S. K. Upadhyay *et al.* (19).

References and Notes

1. G. Prinz, *Phys. Today* **48**, 58 (1995).
2. M. B. Stearns, *J. Magn. Magn. Mater.* **5**, 167 (1977).
3. See, for example, *Polarized Electrons in Surface Physics*, R. Feder, Ed. (World Scientific, Singapore, 1985).
4. P. M. Tedrow and R. Meservey, *Phys. Rep.* **238**, 173 (1994).
5. A. F. Andreev, *Zh. Eksp. Teor. Fiz.* **46**, 1823 (1964) [*Sov. Phys.–J. Exp. Theor. Phys.* **19**, 1228 (1964)].
6. L. Ranno, A. Barry, J. M. D. Coey, *J. Appl. Phys.* **81**, 5774 (1997).
7. D. Kämper, W. Schmitt, G. Güntherodt, R. Gambino, R. Ruf, *Phys. Rev. Lett.* **59**, 2788 (1987).
8. K. Schwarz, *J. Phys. F* **16**, L211 (1986).
9. J. M. MacLaren, X.-G. Zhang, W. H. Butler, *Phys. Rev. B* **56**, 11827 (1997).
10. Yu V. Sharvin, *Zh. Eksp. Teor. Fiz.* **48**, 984 (1965) [*Sov. Phys.–J. Exp. Theor. Phys.* **21**, 655 (1965)].
11. G. E. Blonder, M. Tinkham, T. M. Klapwijk, *Phys. Rev. B* **25**, 4515 (1982).
12. M. J. M. de Jong and C. W. J. Beenakker, *Phys. Rev. Lett.* **74**, 1657 (1995).
13. G. E. Blonder and M. Tinkham, *Phys. Rev. B* **27**, 112 (1983).
14. J. S. Moodera, J. Nowak, R. J. M. van de Veerdonk, *Phys. Rev. Lett.* **80**, 2941 (1998).
15. G. A. Prinz and J. J. Krebs, *Appl. Phys. Lett.* **39**, 397 (1981).
16. R. A. de Groot, F. M. Moeller, P. G. van Eugen, K. H. J. Buschow, *Phys. Rev. Lett.* **50**, 2024 (1983).
17. V. G. Harris, unpublished data.
18. Materials synthesis of LSMO thin films was the same as for La$_{0.7}$Ca$_{0.3}$MnO$_3$ [P. R. Broussard, S. B. Qadri, V. M. Browning, V. C. Cestone, *Appl. Surf. Sci.* **115**, 80 (1997).
19. S. K. Upadhyay *et al.*, *Phys. Rev. Lett.*, in press.
20. J.M.B. acknowledges support of this research by the Office of Naval Research (ONR contracts N0001496WX20507 and N00173-98-1-G004). B.N. and T.A. acknowledge the American Society for Engineering Education and National Research Council Postdoctoral Fellowships, respectively. Work at the Massachusetts Institute of Technology was supported by ONR contract N00014-92-J-1847 and ONR AASERT contract N00014-93-1-1204. We also acknowledge T. Clinton, G. Prinz, G. Deutscher, I. Mazin, M. Johnson, and K. Hathaway for useful discussions, and J. Claassen for technical assistance.

15 June 1998; accepted 1 September 1998

Table 1. Summary of experimental results with Andreev reflection to determine the P_C at E_F of several FM metals. The number of point contact adjustments is indicated by N. Each adjustment represents a distinct point contact junction and an independent determination of P_C. Columns 5 and 6 represent a comparison between the previously measured P_T (4) and the value of P_C from the measured $G(0)/G_n$ with Eq. 6, respectively.

Material studied	Point	Base	N	P_T (%)	P_C (%)
NiFe	Nb	Ni$_{0.8}$Fe$_{0.2}$ film	14	25 ± 2	37 ± 5
Co	Nb	Co foil	7	35 ± 3	42 ± 2
Fe	Ta	Fe film	12	40 ± 2	45 ± 2
	Fe	Ta foil	14		46 ± 2
	Nb	Fe film	4		42 ± 2
	Fe	V crystal	10		45 ± 2
Ni	Nb	Ni foil	4	23 ± 3	46.5 ± 1
	Nb	Ni film	5		43 ± 2
	Ta	Ni film	8		44 ± 4
NiMnSb	Nb	NiMnSb film	9	–	58 ± 2.3
LSMO	Nb	La$_{0.7}$Sr$_{0.3}$MnO$_3$ film	14	–	78 ± 4.0
CrO$_2$	Nb	CrO$_2$ film	9	–	90 ± 3.6